ATR promotes mTORC1 activation via de novo cholesterol synthesis in p16-low cancer cells

Naveen Kumar Tangudu[1,2], Zhentai Huang[1,2], Richard Fang[2], Raquel Buj[1,2], Apoorva Uboveja[1,2], Aidan R. Cole[1,2], Cassandra Happe[2], Mai Sun[2], Stacy L. Gelhaus[1,3], Matthew L. MacDonald[2,4], Nadine Hempel[2,5], Nathaniel W. Snyder[6], and Katherine M. Aird[1,2*]

[1]Department of Pharmacology & Chemical Biology, University of Pittsburgh School of Medicine, Pittsburgh, PA

[2] UPMC Hillman Cancer Center, University of Pittsburgh School of Medicine, Pittsburgh, PA

[2] Health Sciences Mass Spectrometry Core, University of Pittsburgh School of Medicine, PA, USA

[3] Department of Pharmacology and Chemical Biology and Health Sciences Mass Spectrometry Core, University of Pittsburgh School of Medicine, PA, USA

[4] Department of Psychiatry, University of Pittsburgh School of Medicine, Pittsburgh, PA, USA.

[5] Division of Hematology/Oncology, Department of Medicine, University of Pittsburgh School of Medicine, Pittsburgh, PA

[6] Department of Cardiovascular Sciences, Aging + Cardiovascular Discovery Center, Lewis Katz School of Medicine, Temple University, Philadelphia, PA

* Corresponding Author
Katherine M. Aird, PhD
Associate Professor
5051 Centre Ave.
Office: 2041; Lab: 2050
Pittsburgh, PA 15213
412-648-4823
katherine.aird@pitt.edu

Running title: ATR promotes mTORC1 via cholesterol

Keywords: metabolism; cell cycle; lanosterol synthase; statins

ABSTRACT

DNA damage and cellular metabolism are intricately linked with bidirectional feedback. Two of the main effectors of the DNA damage response and control of cellular metabolism are ATR and mTORC1, respectively. Prior work has placed ATR upstream of mTORC1 during replication stress, yet the direct mechanism for how mTORC1 is activated in this context remain unclear. We previously published that p16-low cells have mTORC1 hyperactivation, which in part promotes their proliferation. Using this model, we found that ATR, but not ATM, is upstream of mTORC1 activation via *de novo* cholesterol synthesis and is associated with increased lanosterol synthase (LSS). Indeed, p16-low cells showed increased cholesterol abundance. Additionally, knockdown of either ATR or LSS decreased mTORC1 activity. Decreased mTORC1 activity due to ATR knockdown was rescued by cholesterol supplementation. Finally, using both LSS inhibitors and multiple FDA-approved *de novo* cholesterol synthesis inhibitors, we found that the *de novo* cholesterol biosynthesis pathway is a metabolic vulnerability of p16-low cells. Together, our data provide new evidence coupling the DNA damage response and cholesterol metabolism and demonstrate the feasibility of using FDA-approved cholesterol-lowering drugs in tumors with loss of p16.

INTRODUCTION

mTORC1 is a central nutrient sensor (Saxton and Sabatini, 2017). A plethora of signaling and metabolic pathways feed into mTORC1, which activate both transcriptional and translational programs, allowing for cell growth in addition to cell proliferation. We previously published that loss of the tumor suppressor p16 leads to mTORC1 hyperactivation and cellular proliferation in both normal cells and cancer, and this axis is a metabolic vulnerability of tumors with low expression of p16 (termed here p16-low tumors) (Buj et al., 2019). The mechanism underlying how p16 loss enhances mTORC1 activity in our model is not yet understood. Moreover, specific therapies to target p16-low tumors do not yet exist.

The DNA damage response (DDR) plays an important role in maintaining genome stability during oncogenic stress (Jeggo et al., 2016), and DDR and metabolism are linked (Cucchi et al., 2021; Turgeon et al., 2018). One common mechanism whereby cancers hijack DDR is upregulation of ATR and/or ATM (Weber and Ryan, 2015). While activation of these pathways in normal cells leads to a cell cycle arrest to allow for DNA damage repair, cancers often have other cell cycle or DDR alterations that allow for continued proliferation even in the presence of activated ATR/ATM (Maréchal and Zou, 2013). Indeed, many cancers are often reliant on these proteins for continued proliferation, and ATR and ATM inhibitors are in clinical trials for a variety of malignancies (Priya et al., 2023). Both ATR and ATM have roles in metabolism, which may promote cancer phenotypes, including nutrient uptake and nucleotide synthesis (Aird et al., 2015; Chen et al., 2020; Dahl and Aird, 2017; Diehl et al., 2022; Huang et al., 2023). It is therefore unsurprising that studies have previously linked both ATR and ATM to the nutrient sensor mTORC1 in a bidirectional fashion (Alexander et al., 2010; Danesh Pazhooh et al., 2021; Lamm et al., 2020; Ma et al., 2018).

However, whether the DDR promotes specific metabolic rewiring to directly enhance mTORC1 signaling remains unknown.

Cholesterol is a key component of the plasma membrane, but also plays important roles in cancer progression through both cell-intrinsic and cell-extrinsic effects (Liu et al., 2023). Cholesterol metabolism is often upregulated in cancer through either *de novo* synthesis and/or increased uptake. The *de novo* synthesis pathway is a multi-step process starting with acetyl-CoA and progressing through the mevalonate pathway including conversion of HMG-CoA to mevalonate by the rate limiting enzyme HMG-CoA reductase and then cholesterol synthesis via squalene and lanosterol leading to cholesterol (Shi et al., 2022). Prior work has shown that cholesterol directly activates mTORC1 via LYCHOS at lysosomes (Castellano et al., 2017; Davis et al., 2021; Lim et al., 2019; Shin et al., 2022). Cholesterol has also been linked to genome instability, yet it has been placed upstream of DNA damage accumulation (Liu et al., 2023).

Here we found that loss of p16 corresponds to DNA damage accumulation and both ATR and ATM activation. We determined that ATR is upstream of mTORC1 in this model, and this was independent of Chk1. Using an unbiased proteomics approach and cross-comparing with publicly available datasets of mTORC1 regulators, we identified the *de novo* cholesterol synthesis enzyme lanosterol synthase (LSS) as a mediator between ATR and mTORC1 activation. Finally, we found that loss of p16 sensitizes cells to a variety of *de novo* cholesterol synthesis inhibitors, indicating the utility of these FDA-approved drugs in the 50% of human cancers with loss of p16 expression. Together, our data demonstrate the link between ATR and mTORC1 via cholesterol synthesis and provide proof-of-concept that this is a targetable axis in tumors with either low p16 expression or increased ATR activation.

RESULTS

Loss of p16 is associated with increased DNA damage accumulation and ATR/ATM signaling

We previously published that loss of p16 suppresses oncogene-induced senescence in part via increased nucleotide metabolism (Buj et al., 2019). One of the hallmarks of senescence is increased DNA damage accumulation (Bartkova et al., 2006; Di Micco et al., 2006). To our surprise, we found that cells with p16 knockdown, which failed to senesce (Buj et al., 2019), had even further increased markers of DNA double strand breaks (DSBs) (**Fig. S1A-C**). As p16 loss occurs in 50% of cancers, we aimed to determine whether this also occurred in cancer cell line models. Indeed, knockdown or knockout of p16 increased markers of DSBs (**Fig. 1A-B and S1D-G**). One of the markers of DBSs, γH2AX, is phosphorylated by ATR or ATM. Indeed, we observed increased phosphorylation of ATR/ATM substrates p-Chk1 and p-Chk2 in multiple cell lines upon p16 knockdown (**Fig. 1C and S1F**). Analysis of RNA-Seq data demonstrated a positive enrichment of the signature related to the G2M checkpoint (**Fig. 1D**), which is associated with ATM/ATR activation. Finally, using melanoma patient samples from TCGA, we found that homozygous deletion of *CDKN2A*, the locus encoding p16, correlated with increased p-Chk1 along with other proteins involved in DNA damage response and repair (**Fig. 1E**). Together, these data demonstrate that loss of p16 expression promotes DNA damage accumulation that corresponds with ATR/ATM pathway activation.

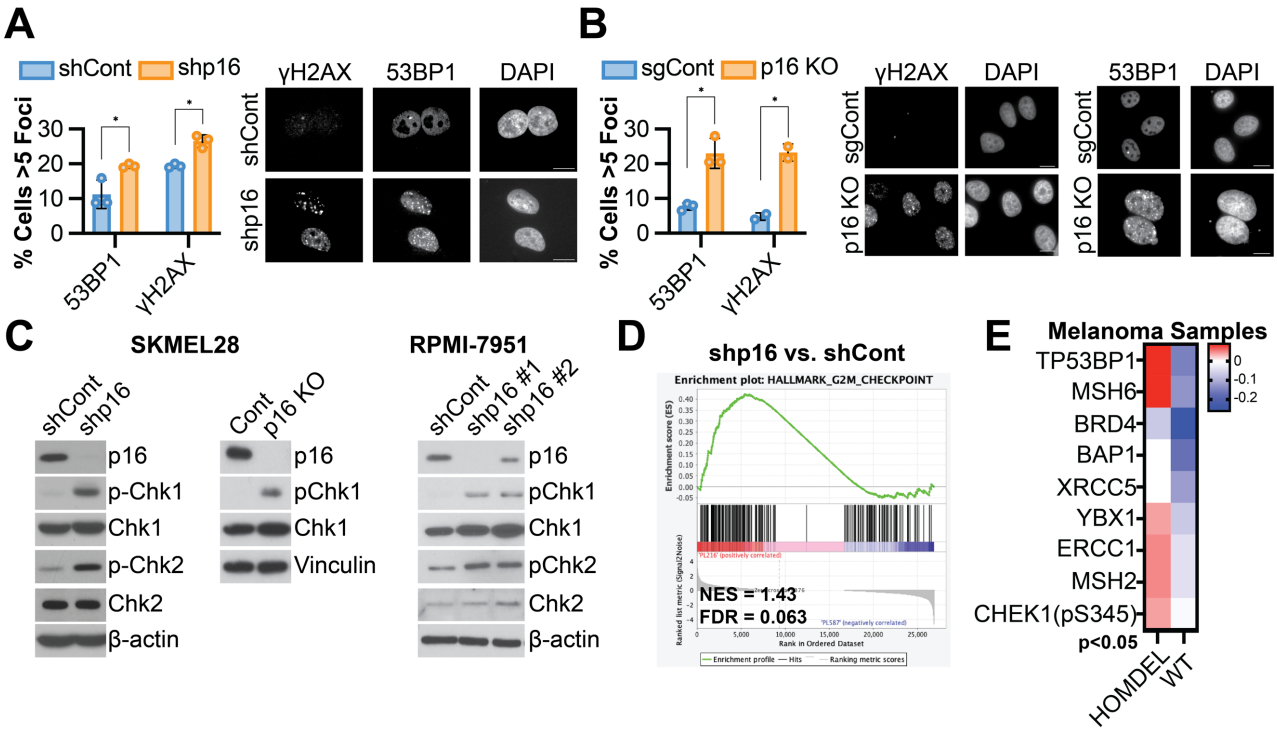

Figure 1. p16 knockdown increases DNA damage accumulation and activation of the ATR/ATM pathway. (A) SKMEL28 melanoma cells were transduced with a lentivirus expressing a short hairpin targeting GFP (shCont) or p16 (shp16), and DNA damage foci were assessed by immunofluorescence. Representative data from 8 independent experiments. **(B)** SKMEL28 melanoma cells were transduced with a guide RNA targeting p16 (p16 KO). Details on controls in Methods. DNA damage foci were assessed by immunofluorescence. Representative data from 3 independent experiments. **(C)** The indicated western blots were performed in SKMEL28 and RPMI-7951 melanoma cells. β-actin or vinculin were used as loading controls. Representative data from 2-3 independent experiments. **(D)** Gene Set Enrichment Analysis of RNA-Seq from SKMEL28 melanoma cells in (A) show positive enrichment of G2M checkpoint signature in shp16 cells. **(E)** RPPA results from Melanoma patient samples show upregulation of proteins related to the DNA damage response and repair in tumors with homozygous deletion of the *CDKN2A* locus compared to intact *CDKN2A* locus (all proteins p<0.05). Graphs represent mean ± SD. T-test. *p<0.05

ATR signaling downstream of p16 loss promotes mTORC1 activity

We previously published that loss of p16 activates mTORC1 signaling (Buj et al., 2019), and prior publications have put ATM or ATR activation upstream of mTORC1 (Alexander et al., 2010; Lamm et al., 2020). To determine whether ATR/ATM pathway activation and mTORC1 signaling are linked, we knocked down either ATR or ATM and assessed mTORC1 activity using S6K phosphorylation as a readout. Interestingly, knockdown of ATR robustly decreased S6K phosphorylation, whereas ATM knockdown only modestly decreased p-S6K (**Fig. 2A and S2A**). Similar results

were observed with an ATR inhibitor at a very low concentration for only 30 minutes, whereas the ATM inhibitor had no effect (**Fig. 2B and S2B**). These data demonstrated that ATR activity affects mTORC1. To delineate whether this is through ATR's activation of Chk1, we also knocked down or inhibited Chk1. Neither knockdown nor inhibition of Chk1 robustly decreased S6K phosphorylation (**Fig. S2C-D**), demonstrating that ATR-mediated downregulation of mTORC1 is likely independent of this key downstream ATR substrate. Finally, inhibition of mTORC1 signaling using Torin 1 did not decrease Chk1 phosphorylation (**Fig. 2C**). Interestingly, Poly-Seq analysis of shp16 cells with knockdown of ATR or RPTOR (a part of the mTOR complex 1) demonstrated ~50% overlap of transcripts that were downregulated when the heavy polysome fraction to total RNA (**Fig. 2D and Table S1**). Together with our western blot analysis, these results suggest that ATR is upstream of mTORC1 in p16-low cells, leading to changes in translation.

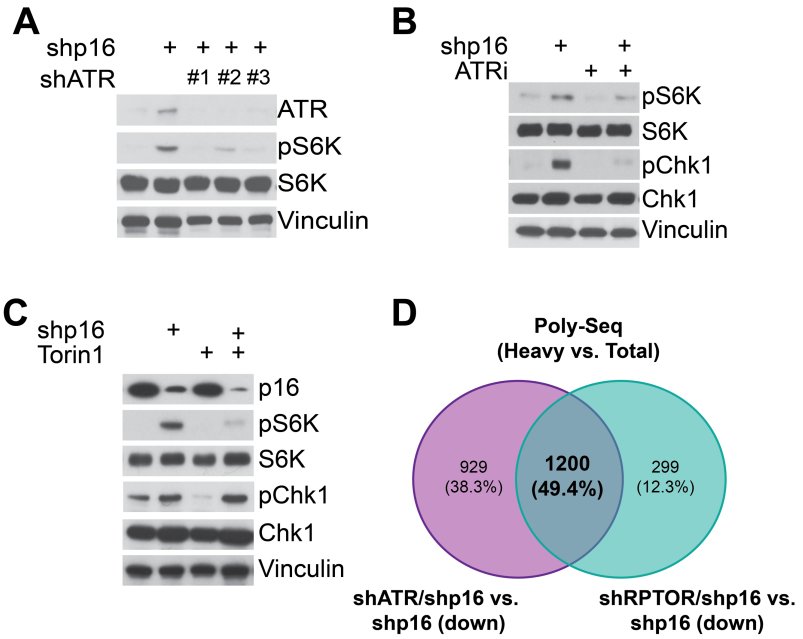

Figure 2. ATR is upstream of mTORC1 in p16 knockdown cells. SKMEL28 melanoma cells were transduced with a lentivirus expressing a short hairpin targeting GFP or p16 (shp16). **(A)** shp16 cells were transduced with a lentivirus expressing a short hairpin targeting GFP or ATR (shATR), and pS6K was assessed by western blotting. Vinculin was used as a loading control. **(B)** Cells were treated for 30min with 63nM VE822 ATR inhibitor (ATRi), and the indicated proteins were assessed by western blotting. Vinculin was used as a loading control. **(C)** Cells were treated for 10min with 250nM of the mTORC1 inhibitor Torin1, and the indicated proteins were assessed by western blotting. Vinculin was used as a loading control. **(D)** Analysis of heavy ribosome fraction vs. total mRNA in the indicated cells.

ATR affects lanosterol synthase and promotes mTORC1 activation via cholesterol

Since our data show that ATR is upstream of mTORC1 activity (**Fig. 2**) but no direct link between ATR and mTORC1 is known, we next aimed to understand the mechanism that couples ATR activity to mTORC1. We cross-compared proteomics data of shp16 cells with knockdown of ATR (**Table S2**) to a publicly available dataset of mTORC1 regulators (Condon et al., 2021). This resulted in 17 potential upstream mTORC1 regulators (**Fig. 3A**). Of these, only 9 were specific to shp16 cells. The one with the most significant changes was lanosterol synthase (LSS) (**Fig. 3B-C**), an enzyme that forms the four-ring structure of cholesterol during the conversion of (*S*)-2,3-

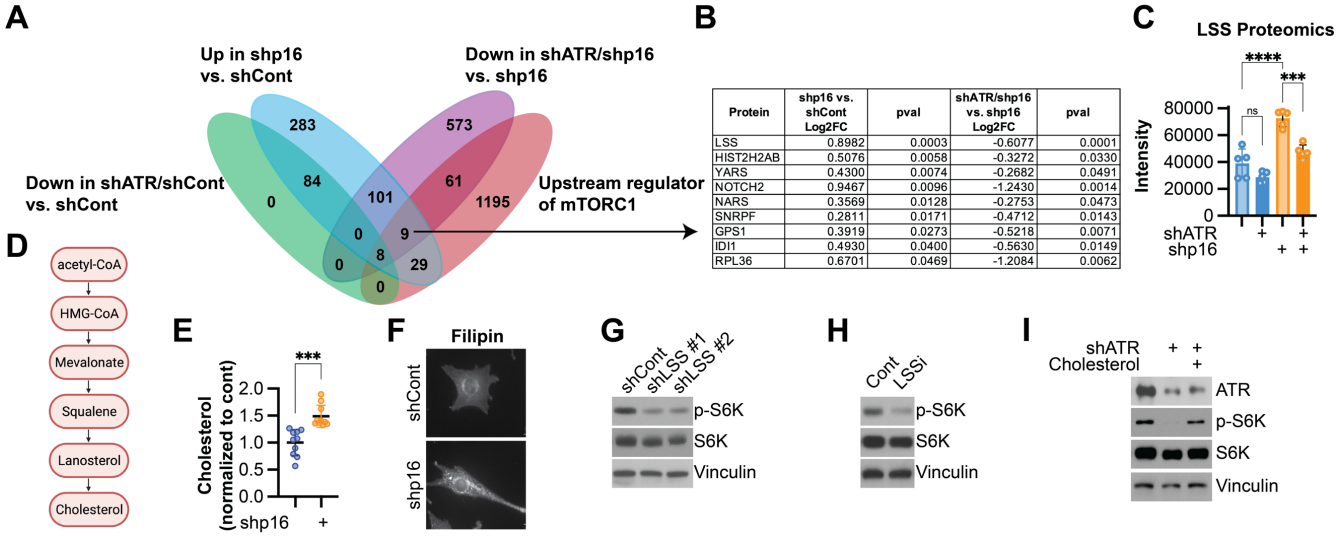

Protein	shp16 vs. shCont Log2FC	pval	shATR/shp16 vs. shp16 Log2FC	pval
LSS	0.8982	0.0003	-0.6077	0.0001
HIST2H2AB	0.5076	0.0058	-0.3272	0.0330
YARS	0.4300	0.0074	-0.2682	0.0491
NOTCH2	0.9467	0.0096	-1.2430	0.0014
NARS	0.3569	0.0128	-0.2753	0.0473
SNRPF	0.2811	0.0171	-0.4712	0.0143
GPS1	0.3919	0.0273	-0.5218	0.0071
IDI1	0.4930	0.0400	-0.5630	0.0149
RPL36	0.6701	0.0469	-1.2084	0.0062

Figure 3. ATR affects lanosterol synthase and promotes mTORC1 activity in p16 knockdown cells via cholesterol. (A-I) SKMEL28 cells were transduced with lentivirus expressing shRNA targeting p16 (shp16) or control (shCont). **(A)** Venn diagram comparing proteomics data with publicly available dataset of mTORC1 regulators. **(B)** Nine hits were found in the cross-comparison from **(A)**. **(C)** LSS protein abundance in the indicated groups. **(D)** Simplified pathway of *de novo* cholesterol synthesis. **(E)** Cholesterol abundance was assessed by filipin staining and analysis of intensity using ImageJ. One of two independent experiments. **(F)** Representative images from filipin staining. **(G)** shp16 SKMEL28 cells were transduced with lentivirus expressing shRNA targeting LSS (shLSS #1 and #2), and p-S6K/S6K was assessed by western blotting. Vinculin was used as a loading control. One of four independent experiments. **(H)** shp16 SKMEL28 cells were treated with 2.5μM LSS inhibitor (LSSi) Ro 48-8071 for 24h, and p-S6K/S6K was assessed by western blotting. Vinculin was used as a loading control. One of three independent experiments. **(I)** shp16 SKMEL28 cells were transduced with lentivirus expressing shRNA targeting ATR (shATR) with or without treatment with 50μM cholesterol for 24h, and p-S6K/S6K was assessed by western blotting. Vinculin was used as a loading control. One of two independent experiments. Graphs represent mean ± SD. T-test or one-way ANOVA. ***p<0.005, ****p<0.001, ns = not significant

epoxysqualene to lanosterol in the *de novo* cholesterol synthesis pathway (**Fig. 3D**). Indeed, prior work has determined that cholesterol directly activates mTORC1 (Castellano et al., 2017; Davis et al., 2021; Lim et al., 2019; Shin et al., 2022). Consistent with our proteomics data, we found that gene sets related to cholesterol synthesis were increased in both cell lines with p16 knockdown and patients with low *CDKN2A* expression (**Fig. S3A**), and cholesterol abundance was increased in cells with p16 knockdown (**Fig. 3E-F and S3B-C**). Notably, we observed increased puncta in shp16 cells (**Fig. 3F and S3B-C**), suggesting differential localization or storage of cholesterol in these cells. Consistent with the notion that LSS is upstream of mTORC1 in these cells, knockdown or inhibition of LSS in shp16 cells decreased S6K phosphorylation (**Fig. 3G-H and S3D-E**). Knockdown of ATR in shp16 cells supplemented with cholesterol rescued S6K phosphorylation (**Fig. 3I**), suggesting the observed increase in mTORC1 activity downstream of ATR is in part via cholesterol reprogramming. Together, these data indicate that ATR is associated with LSS expression and cholesterol abundance, which promotes mTORC1 activity.

Cholesterol is a metabolic vulnerability of p16-low cancers

We previously published that p16-low cancer cells are sensitive to inhibition of mTORC1 (Buj et al., 2019), suggesting that they rely on this pathway for proliferation and/or survival. Since cholesterol directly activated mTORC1 in p16-low cells (**Fig. 3**), we reasoned that this may be a targetable vulnerability of these cells. Indeed, LSS knockdown or inhibition by Ro 48-8071 decreased proliferation and increased cell death in p16 knockdown cells (**Fig. 4A-C and S4A**). We also observed increased sensitivity of these cells to three FDA-approved HMG-CoA reductase inhibitors atorvastatin, lovastatin, and mevastatin (**Fig. 4D and S4B**). Finally, using data from DepMap, we found that cutaneous melanoma cells with low CDKN2A expression are more

sensitive to statins (**Fig. S4C**). Together, these data indicate the utility of FDA-approved cholesterol lowering drugs for cells with low p16 expression.

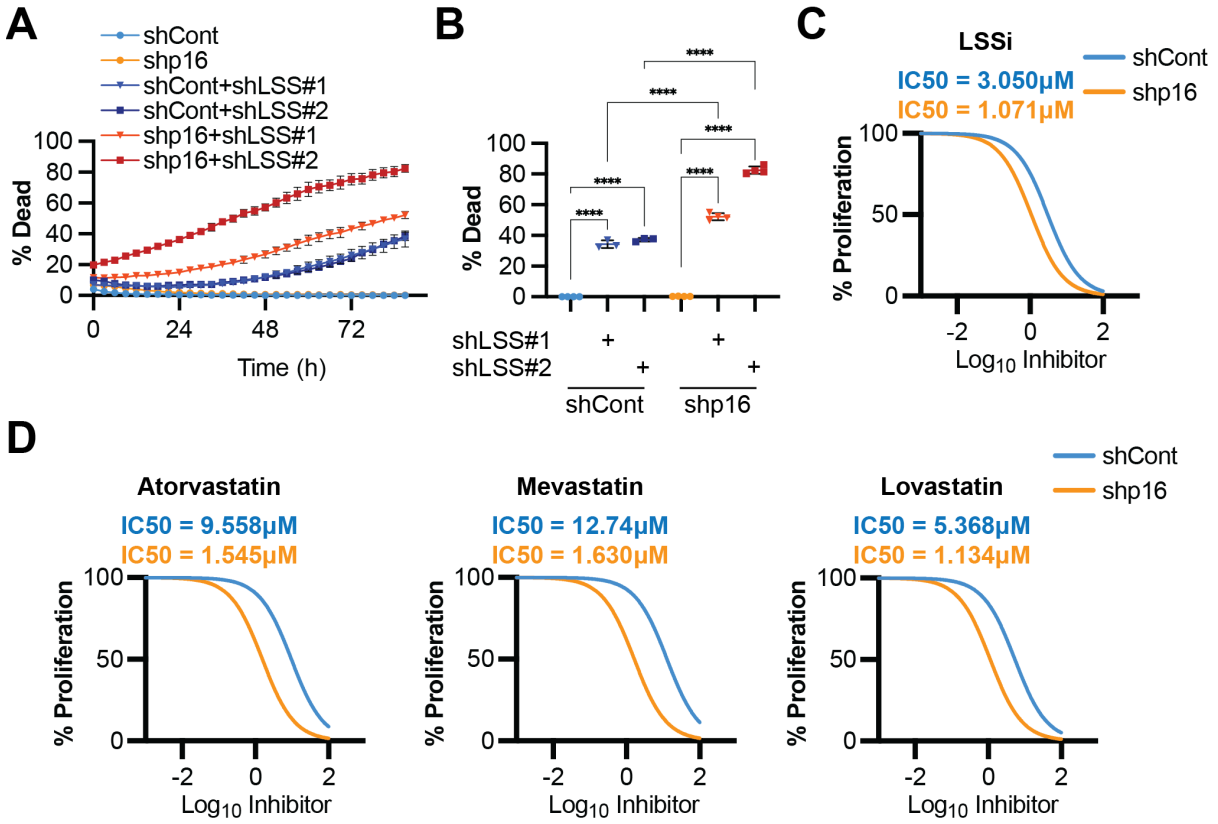

Figure 4. *De novo* cholesterol synthesis inhibitors are a metabolic vulnerability of p16-low cells. (A-D) SKMEL28 cells were transduced with lentivirus expressing shRNA targeting p16 (shp16) or control (shCont). **(A)** Cells were transduced with lentivirus expressing shRNA targeting LSS (shLSS), and cytotoxicity was assessed using Incucyte Cytotox reagent. One of three independent experiments is shown. **(B)** Same as **(A)** but % death and endpoint is shown. One of three independent experiments is shown. Graph represents mean ± SD. One-way ANOVA. ****p<0.001 **(C)** Cells were treated with the LSS inhibitor (LSSi) Ro 48-8071, and proliferation was assessed by crystal violet staining. One of three independent experiments is shown. **(D)** Cells were treated with the de novo cholesterol synthesis inhibitors atorvastatin, mevastatin, and lovastatin, and proliferation was assessed by crystal violet staining. One of three independent experiments is shown.

DISCUSSION

We previously published that p16 loss increases mTORC1 activation (Buj et al., 2019). Here, we identified a mechanism of mTORC1 activation in this context via ATR-mediated *de novo* cholesterol synthesis via lanosterol synthase (LSS). These results establish a link between the DNA damage response and cholesterol signaling. The observed cholesterol rewiring creates a metabolic vulnerability of p16-low cells that is therapeutically targetable using both LSS inhibitors and statins, suggesting that *de novo* cholesterol synthesis inhibitors may provide therapeutic benefit for the ~50% of human tumors with low p16/*CDKN2A* expression.

We found that knockdown of p16 increased markers of DNA double strand breaks and induced activation of the ATR/ATM pathway (**Fig. 1**). The direct mechanism of DNA damage in this context is still unknown. Cell cycle disruption is known to promote DNA replication stress and DNA damage (Gaillard et al., 2015; Primo and Teixeira, 2019). Indeed, our work is consistent with prior studies demonstrating that loss of p16 increases DNA damage (Fung et al., 2013; Tramontano et al., 2020), and loss of p16 has been shown to sensitize cells to UV-induced DNA damage (Sarkar-Agrawal et al., 2004) and telomeric damage during aging (Wang et al., 2013). Given prior work in melanocytes showing DNA hyperreplication due to p16 loss (Fung et al., 2013), and the fact that ATR is activated in response to ssDNA during replication stress (Saldivar et al., 2017), it seems likely that S-phase driven by p16 loss is via this pathway. However, others have found that DNA damage due to RB1 loss, which is downstream of p16, is in part due to oxidative stress (Marshall et al., 2019). Studies have also found that RB1 loss decreases DNA repair (Manickavinayaham et al., 2020; Vélez-Cruz et al., 2016), although p16 has context-dependent effects on DNA repair pathways (Dok et al., 2016; Dok et al., 2014; Molkentine et al., 2022). We previously found that p16 knockdown increases mTORC1 activity in a RB1-independent manner (Buj and Aird, 2019;

Buj et al., 2019). Thus, it is possible that the mechanisms of RB1 loss do not phenocopy those of p16 loss. Additional studies are required to more deeply probe the mechanism of DNA damage accumulation in cells without p16 expression and determine whether this is due to cell cycle dysregulation or other mechanisms.

There is a bidirectional cross-talk between mTORC1 and DNA damage. Interestingly, most studies have placed mTORC1 upstream of DNA damage (Danesh Pazhooh et al., 2021; Ma et al., 2018), with only a handful demonstrating that ATR or ATM are upstream of mTORC1 activation (Alexander et al., 2010; Lamm et al., 2020). One prior report found that replication stress, and therefore ATR activity, promotes nuclear mTORC1 activation (Lamm et al., 2020), although no direct mechanism was identified. Here we found that ATR is upstream of mTORC1 (**Fig. 2**), corresponding with increased cholesterol that supports mTORC1 activity (**Fig. 3**). Prior studies have found that DNA damage, replication stress, and ATR activation promotes nucleotide metabolism (Bao et al., 2023; Buisson et al., 2015; Diehl et al., 2022). How these pathways, and in particular ATR, affect cholesterol is less appreciated. We found that ATR affects expression of LSS, an enzyme in *de novo* cholesterol synthesis (**Fig. 3**). How exactly ATR expression and/or activity promotes this pathway remains to be investigated. ATR is generally thought of as a nuclear protein, while LSS is cytoplasmic. However, ATR has also been found in the cytoplasm (Biswas et al., 2022; Hilton et al., 2016; Postigo et al., 2017); therefore, it is possible ATR directly phosphorylates LSS to promotes its activity or stability. This will be the aim of future studies.

Prior work has elegantly shown how cholesterol promotes mTORC1 activity via LYCHOS at the lysosome (Shin et al., 2022). Using filipin staining, we found that intracellular cholesterol has a more punctate pattern in shp16 cells vs. controls (**Fig. 3**). It is possible that these co-localize with lysosomes to promote mTORC1 activity, but future experiments will be needed to confirm this.

The cellular distribution of cholesterol in control and p16 knockdown cells was striking and may also indicate that these cells store cholesterol differently. Recent work has demonstrated that *CDKN2A*/p16 increases lipid droplets and promotes redistribution of polyunsaturated fatty acids (PUFAs) from lipid droplets (Deleye et al., 2020; Minami et al., 2023). What is driving these changes in the lipidome and lipid droplet formation in the context of p16/*CDKN2A*-loss remains an area that needs to be explored.

We found increased cholesterol in p16-low cells (**Fig. 3**), but what this is cholesterol specifically being used for? Cholesterol is a critical component of the plasma membrane but can also lead to increased steroid hormones, vitamin D, and bile acids (Centonze et al., 2022; Liu et al., 2023). We and others have found that p16-low cells proliferate faster than controls (Buj and Aird, 2019; Fung et al., 2013; Tangudu et al., 2023), and thus likely need more membranes during cell division. Additionally, both steroids and bile acids promote pro-tumorigenic signaling pathways (Centonze et al., 2022; Liu et al., 2023). Bile acids also induce ROS (Orozco-Aguilar et al., 2021), which may induce and/or reinforce the DNA damage observed in p16-low cells (**Fig. 1**). Together, this likely indicates that cholesterol metabolism may have pleotropic effects on these cells.

De novo cholesterol synthesis is a well-drugged metabolic pathway. Indeed, due to roles of cholesterol in heart disease, a variety of FDA-approved drugs exist to lower cholesterol levels, including statins, which are HMG-CoA reductase inhibitors. For the reasons described above, cancer cells often upregulate cholesterol synthesis, which can be targeted using cholesterol-lowering drugs (Liu et al., 2023). While some epidemiological data have demonstrated that the use of statins is associated with a reduction in risk from cancer-related death, other studies have shown little to no effect (Longo et al., 2020). We found that loss of p16 promotes hypersensitivity to these agents (**Fig. 4**). Thus, it is possible that *CDKN2A*/p16 status needs to be considered when

stratifying patients for statin therapy, although more experiments including *in vivo* pre-clinical models are needed to solidify these results.

In summary, this study couples the DNA damage response via ATR signaling to *de novo* cholesterol synthesis, which activates mTORC1. We also find that *de novo* cholesterol synthesis is a metabolic vulnerability of p16-low cancer cells that can be exploited using FDA-approved statins. Given that *CDKN2A*/p16 is mutated or its expression is downregulated or lost in ~50% of all human cancers, these results may have implications for a large subset of cancers. Our study also raises the intriguing possibility of using dietary interventions to augment other standard-of-care therapies for these patients.

SUPPLEMENTAL FIGURES

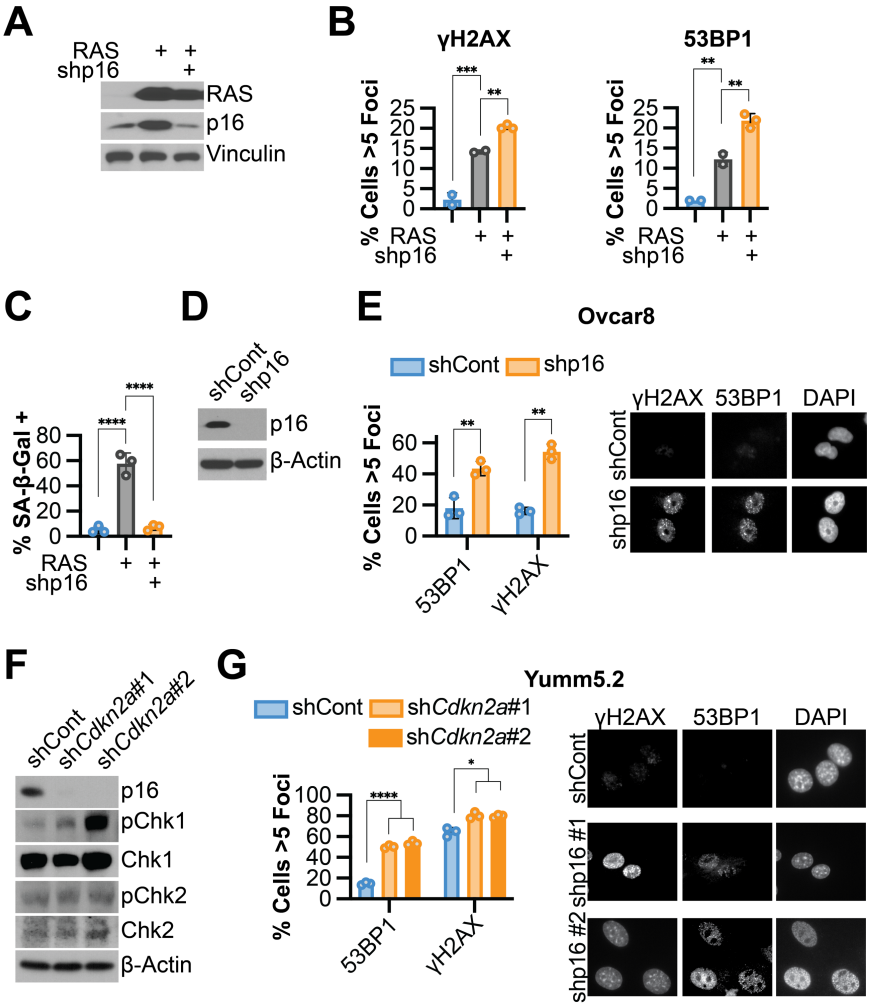

Supplemental Figure 1. Knockdown of p16 increases DNA damage foci in normal cells with oncogene induction and cancer cells. Related to Figure 1. (A-C) IMR90 normal human fibroblasts were transduced with retrovirus expressing HRASG12V (RAS) with or without a lentivirus expressing a short hairpin targeting p16 (shp16). **(A)** Western blot of RAS and p16. Vinculin was used as a loading control. One of >10 independent experiments shown. **(B)** DNA damage foci were assessed by immunofluorescence. One of three independent experiments shown. **(C)** Senescence-associated beta-galactosidase (SA-β-Gal) activity. One of >10 independent experiments shown. **(D-E)** Ovcar8 ovarian cancer cells were transduced with a lentivirus expressing a short hairpin targeting GFP (shCont) or p16 (shp16). **(D)** p16 was assessed by western blotting. β-actin was used as a loading control. One of 3 independent experiments. **(E)** DNA damage foci were assessed by immunofluorescence. One of three independent experiments shown. **(F-G)** Yumm5.2 melanoma cells were transduced with a lentivirus expressing a short hairpin targeting GFP (shCont) or two independent hairpins targeting *Cdkn2a* (sh*Cdkn2a*#1 and sh*Cdkn2a*#2). **(F)** The indicated proteins were assessed by western blotting. β-actin was used as a loading control. One of 10 independent experiments. **(G)** and DNA damage foci were assessed by immunofluorescence. One of three independent experiments shown. Graphs represent mean ± SD. T-test or one-way ANOVA. *p<0.05, **p<0.01, ***p<0.005, ****p<0.001

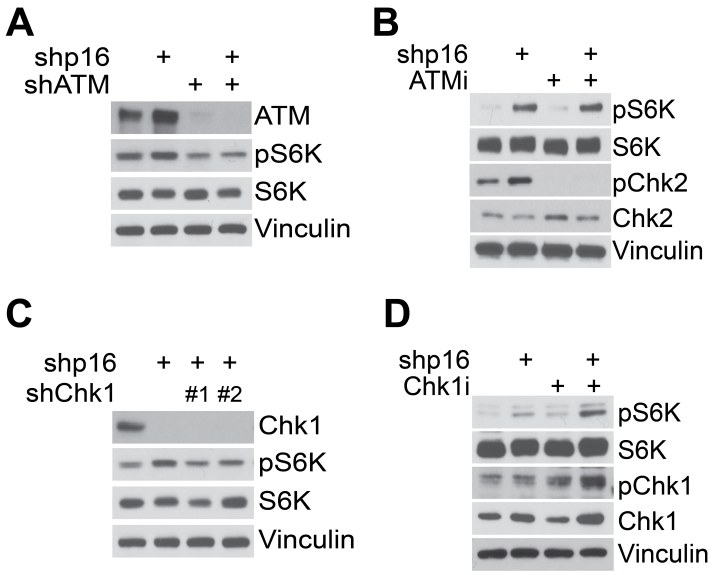

Supplemental Figure 2. Knockdown or inhibition of ATM and Chk1 only modestly downregulated mTORC1 activity. Related to Figure 2. (A-D) SKMEL28 cells were transduced with lentivirus expressing shRNA targeting p16 (shp16) or control (shCont). **(A)** Cells were transduced with lentivirus expressing shRNA targeting ATM (shATM) or control, and the indicated proteins were assessed by western blotting. Vinculin was used as a loading control. One of three independent experiments is shown. **(B)** Cells were treated with the ATM inhibitor 313nM (ATMi) KU60019 for 30min, and the indicated proteins were assessed by western blotting. Vinculin was used as a loading control. One of three independent experiments is shown. **(C)** Cells were transduced with lentivirus expressing shRNA targeting Chk1 (shChk1) or control, and the indicated proteins were assessed by western blotting. Vinculin was used as a loading control. One of three independent experiments is shown. **(D)** Cells were treated with the Chk1 inhibitor 313nM (Chk1i) LY2603618 for 30min, and the indicated proteins were assessed by western blotting. Vinculin was used as a loading control. One of three independent experiments is shown.

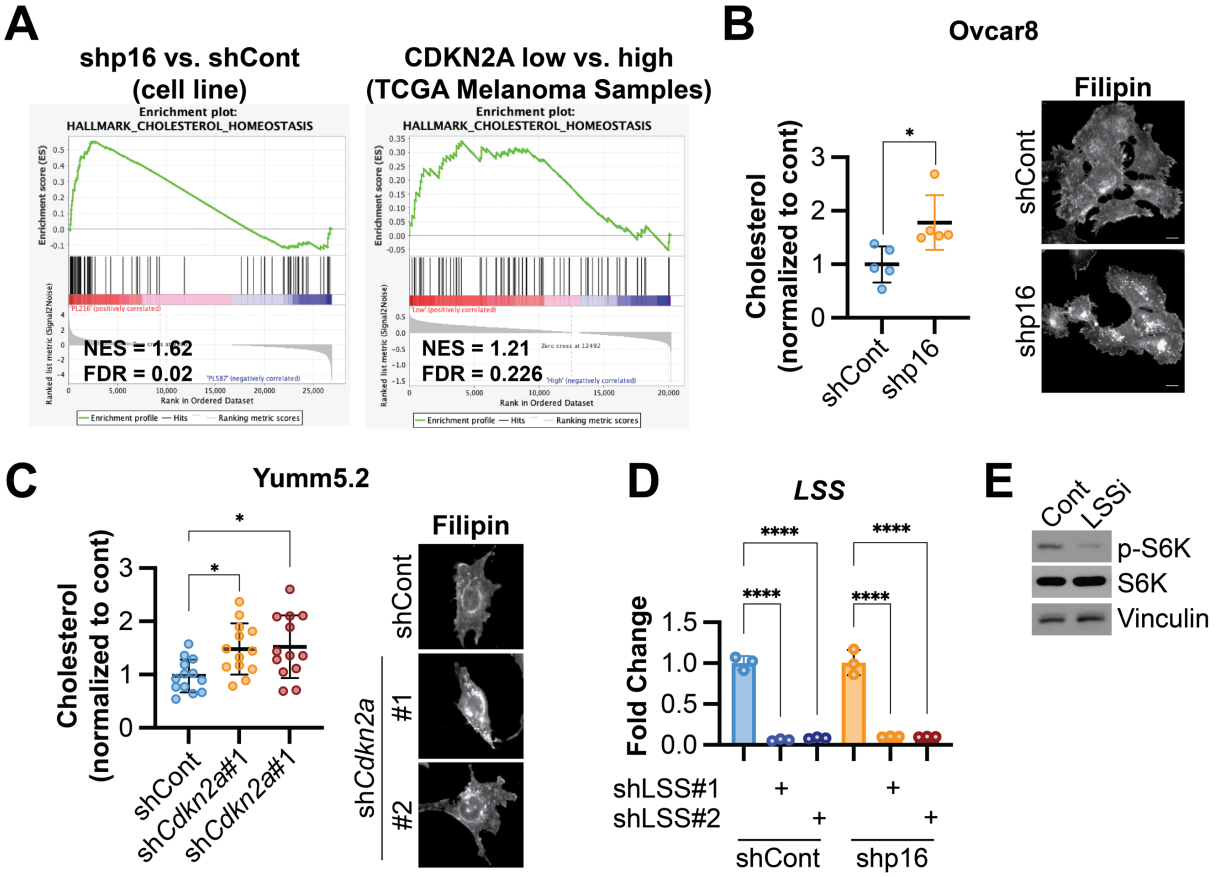

Supplemental Figure 3. Cholesterol signatures are upregulated in shp16 cells and melanoma patients with low *CDKN2A*. Related to Figure 3. (A) Gene Set Enrichment Analysis (GSEA) of SKMEL28 cells with p16 knockdown (left) and Melanoma samples with low CDKN2A expression (right) show enrichment of signatures related to cholesterol. **(B)** Ovcar8 cells were transduced with lentivirus expressing shRNA targeting p16 (shp16) or control (shCont). Cholesterol abundance was assessed by filipin staining and analysis of intensity using ImageJ (left). Representative images from filipin staining (right). **(C)** Yumm5.2 cells were transduced with lentivirus expressing shRNA targeting *Cdkn2a* (sh*Cdkn2a*) or control (shCont). Cholesterol abundance was assessed by filipin staining and analysis of intensity using ImageJ (left). Representative images from filipin staining (right). **(D)** SKMEL28 cells were transduced with lentivirus expression hairpins targeting LSS (shLSS), and *LSS* expression was assessed by RT-qPCR. Knockdown was normalized to respective controls. **(E)** shp16 Ovcar8 cells were treated with 5μM LSS inhibitor (LSSi) Ro 48-8071 for 24h, and p-S6K/S6K was assessed by western blotting. Vinculin was used as a loading control. One of two independent experiments. Graphs represent mean ± SD. T-test. *p<0.05

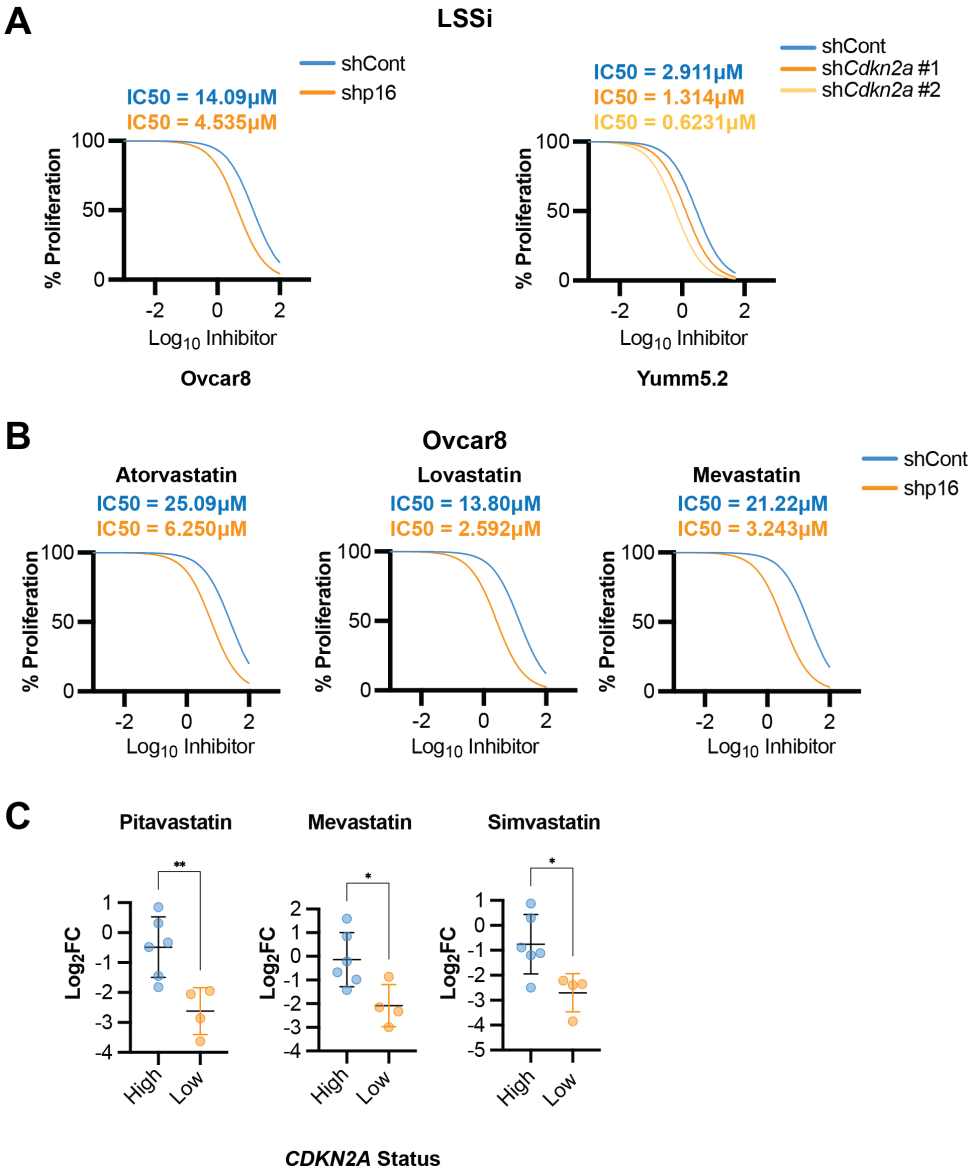

Supplemental Figure 4. *De novo* cholesterol synthesis inhibitors are a metabolic vulnerability of p16-low and Cdkn2a-low cells. (A) Ovcar8 (left) or Yumm5.2 (right) cells were transduced with lentivirus expressing shRNA targeting p16 (shp16) or *Cdkn2a* (sh*Cdkn2a*). Cells were treated for with the LSS inhibitor (LSSi) Ro 48-8071, and proliferation was assessed by crystal violet staining. One of at least 2 independent experiments is shown. **(B)** Ovcar8 cells were treated with the *de* novo cholesterol synthesis inhibitors atorvastatin, mevastatin, and lovastatin, and proliferation was assessed by crystal violet staining. One of at least two independent experiments is shown. **(C)** Increased drug sensitivity from DepMap data of cutaneous melanoma cell lines with high or low *CDKN2A* expression. Data are mean ± SD. T-test. *p<0.05, **p<0.01

Acknowledgements

This work was supported by grants from the National Institutes of Health (R37CA240625 to K.M.A., R01CA259111 to K.M.A. and N.W.S, T32GM133332 to A.R.C., and S10OD023402 and S10OD032141 to S.L.G.), the Melanoma Research Foundation (to R.B.G.), and the Ovarian Cancer Research Alliance (MIG-2023-2-1018 to A.U.).

Author Contributions

Naveen Kumar Tangudu: Investigation, Methodology, Visualization, Writing – Review & Editing. **Zhentai Huang:** Investigation. **Richard Fang:** Investigation, Writing – Review & Editing. **Raquel Buj:** Investigation, Visualization, Writing – Review & Editing. **Aidan Cole:** Investigation, Writing – Review & Editing. **Apoorva Uboveja:** Investigation, Writing – Review & Editing. **Cassandra Happe:** Investigation. **Mai Sun:** Investigation. **Stacy L. Gelhaus:** Methodology, Supervision, Funding Acquisition. **Matthew L. MacDonald:** Methodology, Supervision, Funding Acquisition. **Nadine Hempel:** Writing – Review & Editing**. Nathaniel W. Snyder:** Writing – Review & Editing, Funding Acquisition. **Katherine M. Aird:** Conceptualization, Visualization, Writing – Original Draft, Writing – Review & Editing, Supervision, Project Administration, Funding Acquisition.

Declaration of Interests

All authors declare no competing interests.

Materials and Methods

Cell Lines

SKMEL28, RPMI-7951, and YUMM5.2 cells were purchased from ATCC. Ovcar8 were a kind gift from Dr. Benjamin Bitler (University of Colorado). SKMEL28 cells were cultured in DMEM (Fisher Scientific cat# MT10013CV,) supplemented with 5% Fetal Bovine Serum (BioWest, cat# S1620). RPMI-7951 cells were cultured in MEM (Fisher Scientific cat#MT10009CV) supplemented with 5% Fetal Bovine Serum (BioWest, cat# S1620). OVCAR8 were cultured in RPMI (Fisher Scientific cat#MT10040CV) supplemented with 5% Fetal Bovine Serum (BioWest, cat# S1620). YUMM5.2 cells were cultured in DMEM and Ham's F12 50/50 (Fisher Scientific, cat# MT10092CV,) supplemented with 10% Fetal Bovine Serum (BioWest, cat# S1620) and nonessential amino acids (Corning, cat#25-025-CI). Cells were supplemented with 1% Penicillin/Streptomycin (Fisher Scientific, cat#15-140-122). All cell lines were routinely tested for mycoplasma as described in (Uphoff and Drexler, 2005).

Lentiviral packaging and infection

Lentiviral vectors were packaged using the ViraPower Kit (Invitrogen, cat#K497500) following the manufacturer's instructions. Retrovirus was generated as we have previously published using QNX cells (Buj et al., 2019). Cells were infected with corresponding vectors for 16h and selected for 3 days with 1-3µg/ml puromycin. The plasmids are the following: pBABE-puro-H-RASG12V (Addgene, 39526); pBabe-puro (Addgene, 1764); pLKO.1-shp16 (TRCN0000010482); pLKO.1-shGFP control (Addgene, cat#30323); pLKO.1-shATR (TCRN0000039615, TCRN0000039616); pLKO.1-shATM (TCRN0000038658); pLKO.1-shChk1 (TRCN0000000499, TRCN0000000502); pLKO.1-shRPTOR (TRCN0000039772); pLKO.1-LSS (TRCN0000045481, TRCN0000045482); pLKO.1-shCdkn2a (TRCN0000077816, TRCN0000362595).

Immunofluorescence

Cells were seeded at an equal density on coverslips and fixed with 4% paraformaldehyde. Cells were washed four times with PBS and permeabilized with 0.2% Triton X-100 in PBS for 5min. Cells were blocked for 5 min with 3% BSA/PBS followed by incubation of corresponding primary antibody in 3% BSA/PBS for 1h at room temperature. Cells were washed three times with 1% Triton X-100 in PBS and incubated with secondary antibody in 3% BSA/PBS for 1h at room temperature. Cells were then incubated with 0.15 µg/ml DAPI for 1 min, washed three times with PBS, mounted with fluorescence mounting medium (9 ml of glycerol [BP229-1; Fisher Scientific], 1 ml of 1× PBS, and 10 mg of p-phenylenediamine [PX0730; EMD Chemicals]; pH was adjusted to 8.0–9.0 using carbonate-bicarbonate buffer [0.2 M anhydrous sodium carbonate, 0.2 M sodium bicarbonate]) and sealed. At least 200 cells per coverslip were counted. Primary antibodies: Rabbit anti-53BP1 (Bethyl, Cat # A300-272A, 1:1000), Mouse anti-phospho-Histone H2A.X (Ser139) (Millipore Sigma, Cat#05-636, 1:2000). Secondary antibodies: Fluorescein (FITC)-AffiniPure Donkey Anti-Rabbit (Jackson Immuno, cat# 711-095-152, 1:1000), Cy3 Goat Anti-Rabbit (Jackson Immuno, cat# 111-165-003, 1:5000), Cy3-AffiniPure Donkey Anti-Mouse (Jackson Immuno, cat# 715-165-150, 1:5000).

Western blotting

Cells lysates were collected in 1X sample buffer (2% SDS, 10% glycerol, 0.01% bromophenol blue, 62.5mM Tris, pH 6.8, 0.1M DTT) and boiled to 95°C for 10 min. Protein concentration was determined using the Bradford assay (Bio-Rad, cat#5000006). An equal amount of total protein was resolved using SDS-PAGE gels and transferred to nitrocellulose membranes (Fisher Scientific) at 110mA for 2h at 4°C. Membranes were blocked with 5% nonfat milk or 4% BSA in TBS containing 0.1% Tween-20 (TBS-T) for 1h at room temperature. Membranes were incubated

overnight at 4°C in primary antibodies in 4% BSA/TBS + 0.025% sodium azide. Membranes were washed 4 times in TBS-T for 5 min at room temperature after which they were incubated with HRP-conjugated secondary antibodies (Cell Signaling Technology) for 1 h at room temperature. After washing 4 times in TBS-T for 5 min at room temperature, proteins were visualized on film after incubation with SuperSignal West Pico PLUS Chemiluminescent Substrate (ThermoFisher, Waltham, MA). Primary antibodies: Rabbit anti-p16 INK4A (Cell Signaling Technology, 29271; 1:1000); Phospho-Chk1 (Ser345) (Cell Signaling Technology, Cat# 2348, 1:1000); Mouse anti Chk1 (Cell Signaling Technology, Cat# 2360, 1:1000); Rabbit anti-Phospho-Chk2 (Thr68) (Cell Signaling Technology, Cat# 2197, 1:1000); Rabbit anti-Chk2 (Cell Signaling Technology, Cat# 2662, 1:1000); mouse anti-β-actin (Sigma Aldrich, cat# A1978; 1:10,000); Mouse anti-vinculin (Sigma Aldrich, cat# V9131; 1:10,000); Rabbit anti-ATR (Bethyl, Cat # A300-138A, 1:1000); Rabbit anti- phopsho-p70 S6 Kinase (T389) (Cell Signaling Technology, Cat # 9234, 1:1000); Rabbit anti- p70 S6 Kinase (Cell Signaling Technology, Cat # 2708, 1:1000); Mouse Anti-Ras (BD Biosciences, Cat# 610001, 1:1000). Secondary antibodies: Anti-mouse IgG, HRP-linked (Cell Signaling Technology, 7076; 1:10,000), Anti-Rabbit IgG, HRP-linked (Cell Signaling Technology, 7074; 1:5000).

Analysis of The Cancer Genome Atlas patient data

RPPA Data were extracted from The Cancer Genome Atlas (TCGA) Skin Cutaneous Melanoma Firehose Legacy using cBioportal. Patients were divided based on homozygous deletion (or not) of *CDKN2A*.

RNA isolation, Sequencing, and Analysis

Total RNA was extracted from cells with Trizol (Ambion, cat#15596018) and DNase treated, cleaned and concentrated using Zymo columns (Zymo Research, cat#R1013) following manufacturer's instructions. RNA integrity number (RIN) was measured using BioAnalyzer (Agilent Technologies) RNA 6000 Nano Kit to confirm RIN above 7 for each sample. The cDNA libraries, next generation sequencing, and bioinformatics analysis was performed by Novogene. Raw and processed RNA-Seq data can be found on GEO (GSE243717). Gene set enrichment analysis (GSEA) was performed using the Broad Institute software (http://software.broadinstitute.org/gsea/index.jsp) with the following parameters: (1000 permutations, weighted enrichment statistic, excluding sets larger than 500 and smaller than 15 and using meandiv normalization mode, there were no repeated genes thus collapse mode was not used).

Polysome Profiling and Sequencing

Eight culture plates per condition (~23 million cells per condition) were incubated with harringtonine (2μg/mL) for 2 minutes at 37ºC followed by 5 minutes of cycloheximide (100μg/mL) treatment at 37ºC. Cells were washed twice with PBS after each treatment. Cells were scraped in 600uL of lysis buffer (50mM HEPES, 75mM KCl, 5mM MgCl2, 250mM sucrose, 0.1mg/mL cycloheximide, 2mM DTT, 1% Triton X-100 and 1.3% sodium deoxycholate and 5μl of RNase OUT) on ice. Lysates were rocked for 10 minutes at 4ºC and centrifuged at 3000g for 15 minutes at 4ºC. 400μl of lysates supernatant (cytosolic cell extracts) were layered over cold sucrose gradients (10mM HEPES, 75mM KCl, 5mM MgCl2, 0.5mM EDTA and increasing sucrose concentrations from 20% to 47%). Gradients were centrifuged at 34,000 rpms in a Beckman SW41 rotor for 2h and 40 minutes at 4ºC. After centrifugation, low (0 to 2 ribosomes) and high (>2 ribosomes) polysome fractions were collected in Trizol (1:1) using a density gradient fractionation system (Brandel) equipped with a UA-6 absorbance detector and a R1 fraction collector. RNA was DNase

treated, cleaned, and concentrated using Zymo columns (Zymo Research, cat# R1013). The cDNA libraries, next generation sequencing, and bioinformatics analysis was performed by Novogene. Heavy to total fraction was used to analyze transcripts with decreased translation due to ATR or RPTOR knockdown (**Table S1**).

Proteomics

SKMEL28 cells were homogenized in 50mM TEAB, 5% SDS. Total protein was measured by microBCA (Pierce). 500 µg total protein was digested on S-Trap Midi's (Protifi) per manufacture protocol and desalted on Peptide Desalting Spin Columns (Pierce). Phosphopeptides were enriched on an AssayMAP Bravo (Agilent) with Fe3+ column. LC-TIMS-MS/MS analysis was carried out using a nanoElute UHPLC system (Bruker Daltonics, Bremen, Germany) coupled to the timsTOF Pro mass spectrometer mass spectrometer (Bruker Daltonics), using a CaptiveSpray nanoelectrospray (Bruker Daltonics). Roughly 100 ng of peptide digest or phosphopeptide enrichment was loaded on a capillary C18 column (25 cm length, 75 µm inner diameter, 1.6 µm particle size, 120 Å pore size; IonOpticks, Fitzroy, VIC, AUS). Peptides were separated at 55°C using a 60 min gradient at a flow rate of 300 nL/min (mobile phase A (MPA): 0.1% FA; mobile phase B (MPB): 0.1% FA in acetonitrile). A linear gradient of 2–35% MPB was applied for 60 min, followed by a 5 min wash at 95% MFB before equilibrating the column at 2% MFB for 6 min. The timsTOF Pro was operated in PASEF mode collecting full scan mass spectra from 100 and 1700 *m*/*z*. Ion mobility resolution was set to 0.60–1.60 V·s/cm over a ramp time of 100 ms. Data-dependent acquisition was performed using 10 PASEF MS/MS scans per 1.1 second cycle. Active exclusion time window was set to 0.4 min, and the intensity threshold for MS/MS fragmentation was set to 2.5e4 while low *m*/*z* and singly charged ions were excluded from PASEF precursor selection. MS/MS spectra were acquired via ramped collision energy as function of ion mobility.

The nLC-MS/MS data were analyzed with the MaxQuant software suite (version 2.1.3) (Cox and Mann, 2008). The Andromeda protein identification search engine (Cox et al., 2011) and a Swiss-sProt human protein database (downloaded on November 11, 2022 with 20,403 entries) was utilized with default settings for Orbitrap instruments. The parameters used included a precursor mass tolerance of 20 ppm for the first search and 4.5 ppm for the main search, a product ion mass tolerance of 0.2 Da, and a minimum peptide length of 5 amino acids. Trypsin was set as the proteolytic enzyme with a maximum of two missed cleavages allowed. The enzyme specifically cleaves peptide bonds C-terminal of arginine and lysine if they are not followed by proline. Carbamidomethylation of cysteine was set as a fixed modification. Oxidation of methionine, deamination of both asparagine and glutamine, and acetylation of the protein N-terminus were set as variable modification. Phosphorylation of serine, threonine, and tyrosine was set as a variable modification for phosphopeptides. A 1% false discovery rate (FDR) was used to filter the peptide identification results. The integrated feature intensities provide a relative measure of abundance for each feature at the peptide level and used in all subsequent analyses. Proteomics data can be found in **Table S2**.

Filipin staining and analysis

Cells were cultured on coverslips and fixed with 4% paraformaldehyde. Cells were incubated with 0.1mg/ml filipin III (Cayman Chemical, cat# 70440) for 45min. Coverslips were washed twice with PBS, mounted, and sealed. Abundance was assessed by integrated density of staining using ImageJ and normalized to cell count.

RT-qPCR

RNA was isolated as described above. RNA was retrotranscribed with High-Capacity cDNA Reverse Transcription Kit (Applied Biosystems, cat#4368814) and 20ng of cDNA amplified using the

CFX Connect Real-time PCR system (Bio-Rad) and the PowerUp™ SYBR™ Green Master Mix (Applied Biosystems, cat#A25742) following the manufacturer's instructions. Primers were designed using the Integrated DNA Technologies (IDT) web tool. Conditions for amplification were: 5 min at 95° C, 40 cycles of 10 sec at 95° C and 7 sec at 62° C. The assay ended with a melting curve program: 15 sec at 95° C, 1 min at 70° C, then ramping to 95° C while continuously monitoring fluorescence. Each sample was assessed in triplicate. Relative quantification was determined to multiple reference genes (human: *PSMC4* and *ACTB*) to ensure reproducibility using the delta-delta CT method. Primer sequences: *LSS* F: ACAAGAAAGGTGGTGCTGT, *LSS* R: CATCTCTGGGAACAGGGTATT; *PSMC4* F: TGTTGGCAAAGGCGGTGGCA, *PSMC4* R: TCTCTTGGTGGCGATGGCAT; *ACTB* F: CCAACCGCGAGAAGATGA, *ACTB* R: CCAGAGGCGTACAGGGATAG.

Dependency Map Data

For analysis of sensitivity to statins (using the PRISM Repurposing Primary Screen), cutaneous melanoma cells were characterized as *CDKN2A* high or low based on mRNA expression (Expression Public 23Q2). Cell lines with known *CDKN2A* mutations were excluded.

IncuCyte cytotoxicity assay

Live cell viability was assessed using IncuCyte S3 imaging system (Sartorius). Briefly, cells were seeded in 96 well plate in the presence of 1x Cytotox reagent (cat# ESS4633 or ESS4632; Sartorius), a highly sensitive cyanine nucleic acid dye. Cells were imaged for 3 days with live cell imaging every 3h point. Dead cell quantification was performed using the IncuCyte software.

Senescence-associated β-galactosidase activity assay

Cells were seeded at an equal density 24 h before assay. Cells were fixed for 5 min at room temperature using 2% formaldehyde/0.2% glutaraldehyde in PBS. Cells were then washed twice with 1× PBS and stained with 40 mM Na2H PO4, 150 mM NaCl, 2 mM MgCl2, 5 mM K3Fe(CN)6, 5 mM K4Fe(CN)6, and 1 mg/ml X-gal staining solution overnight at 37°C in a non-CO2 incubator. At least 100 cells per well were counted.

Proliferation assays

An equal number of cells were seeded in multiwell plates, treated with the indicated inhibitors, and cultured for 4-5 days. Proliferation was assessed by fixing the plates for 5 min with 1% para-formaldehyde after which they were stained with 0.05% crystal violet. Wells were destained using 10% acetic acid. Absorbance (590nm) was measured using a spectrophotometer (BioTek Epoch Microplate reader).

Quantification and Statistical Analysis

GraphPad Prism (version 9.0) was used to perform statistical analysis. Point estimates with standard deviations or standard errors were reported, as indicated, and the appropriate statistical test was performed using all observed experimental data. All statistical tests performed were two-sided and p-values < 0.05 were considered statistically significant.

Data Availability Statement

Some of the data generated in this study are publicly available in Gene Expression Omnibus (GEO) at GSE243717. The Poly-Seq data and proteomics data can be found in Table S1 and Table S2.

References

Aird, K.M., Worth, A.J., Snyder, N.W., Lee, J.V., Sivanand, S., Liu, Q., Blair, I.A., Wellen, K.E., and Zhang, R. (2015). ATM couples replication stress and metabolic reprogramming during cellular senescence. Cell reports *11*, 893-901.

Alexander, A., Cai, S.L., Kim, J., Nanez, A., Sahin, M., MacLean, K.H., Inoki, K., Guan, K.L., Shen, J., Person, M.D.*, et al.* (2010). ATM signals to TSC2 in the cytoplasm to regulate mTORC1 in response to ROS. Proceedings of the National Academy of Sciences of the United States of America *107*, 4153-4158.

Bao, W., Zhang, W., Huang, Y., Zhao, Y., Wu, C., Duan, L., Wang, L., and Yan, S. (2023). Protein kinase ATR inhibits E3 ubiquitin ligase CRL4PRL1 to stabilize ribonucleotide reductase in response to replication stress. Cell reports *42*, 112685.

Bartkova, J., Rezaei, N., Liontos, M., Karakaidos, P., Kletsas, D., Issaeva, N., Vassiliou, L.V., Kolettas, E., Niforou, K., Zoumpourlis, V.C.*, et al.* (2006). Oncogene-induced senescence is part of the tumorigenesis barrier imposed by DNA damage checkpoints. Nature *444*, 633-637.

Biswas, H., Zhao, S.J., Makinwa, Y., Bassett, J.S., Musich, P.R., Liu, J.Y., and Zou, Y. (2022). Prolyl Isomerization-Mediated Conformational Changes Define ATR Subcellular Compartment-Specific Functions. Front Cell Dev Biol *10*, 826576.

Buisson, R., Boisvert, J.L., Benes, C.H., and Zou, L. (2015). Distinct but Concerted Roles of ATR, DNA-PK, and Chk1 in Countering Replication Stress during S Phase. Molecular cell *59*, 1011-1024.

Buj, R., and Aird, K.M. (2019). p16: cycling off the beaten path. Molecular & Cellular Oncology *6*, e1677140.

Buj, R., Chen, C.W., Dahl, E.S., Leon, K.E., Kuskovsky, R., Maglakelidze, N., Navaratnarajah, M., Zhang, G., Doan, M.T., Jiang, H.*, et al.* (2019). Suppression of p16 Induces mTORC1-Mediated Nucleotide Metabolic Reprogramming. Cell reports *28*, 1971-1980 e1978.

Castellano, B.M., Thelen, A.M., Moldavski, O., Feltes, M., van der Welle, R.E., Mydock-McGrane, L., Jiang, X., van Eijkeren, R.J., Davis, O.B., Louie, S.M.*, et al.* (2017). Lysosomal cholesterol activates mTORC1 via an SLC38A9-Niemann-Pick C1 signaling complex. Science (New York, NY) *355*, 1306-1311.

Centonze, G., Natalini, D., Piccolantonio, A., Salemme, V., Morellato, A., Arina, P., Riganti, C., and Defilippi, P. (2022). Cholesterol and Its Derivatives: Multifaceted Players in Breast Cancer Progression. Frontiers in oncology *12*, 906670.

Chen, C.-W., Buj, R., Dahl, E.S., Leon, K.E., Varner, E.L., von Krusenstiern, E., Snyder, N.W., and Aird, K.M. (2020). ATM inhibition drives metabolic adaptation via induction of macropinocytosis. bioRxiv, 2020.2004.2006.027565.

Condon, K.J., Orozco, J.M., Adelmann, C.H., Spinelli, J.B., van der Helm, P.W., Roberts, J.M., Kunchok, T., and Sabatini, D.M. (2021). Genome-wide CRISPR screens reveal multitiered

mechanisms through which mTORC1 senses mitochondrial dysfunction. Proceedings of the National Academy of Sciences of the United States of America *118*.

Cox, J., and Mann, M. (2008). MaxQuant enables high peptide identification rates, individualized p.p.b.-range mass accuracies and proteome-wide protein quantification. Nat Biotechnol *26*, 1367-1372.

Cox, J., Neuhauser, N., Michalski, A., Scheltema, R.A., Olsen, J.V., and Mann, M. (2011). Andromeda: a peptide search engine integrated into the MaxQuant environment. J Proteome Res *10*, 1794-1805.

Cucchi, D., Gibson, A., and Martin, S.A. (2021). The emerging relationship between metabolism and DNA repair. Cell Cycle *20*, 943-959.

Dahl, E.S., and Aird, K.M. (2017). Ataxia-Telangiectasia Mutated Modulation of Carbon Metabolism in Cancer. Frontiers in oncology *7*, 291.

Danesh Pazhooh, R., Rahnamay Farnood, P., Asemi, Z., Mirsafaei, L., Yousefi, B., and Mirzaei, H. (2021). mTOR pathway and DNA damage response: A therapeutic strategy in cancer therapy. DNA repair *104*, 103142.

Davis, O.B., Shin, H.R., Lim, C.Y., Wu, E.Y., Kukurugya, M., Maher, C.F., Perera, R.M., Ordonez, M.P., and Zoncu, R. (2021). NPC1-mTORC1 Signaling Couples Cholesterol Sensing to Organelle Homeostasis and Is a Targetable Pathway in Niemann-Pick Type C. Developmental cell *56*, 260-276.e267.

Deleye, Y., Cotte, A.K., Hannou, S.A., Hennuyer, N., Bernard, L., Derudas, B., Caron, S., Legry, V., Vallez, E., Dorchies, E.*, et al.* (2020). CDKN2A/p16INK4a suppresses hepatic fatty acid oxidation through the AMPKα2-SIRT1-PPARα signaling pathway. The Journal of biological chemistry *295*, 17310-17322.

Di Micco, R., Fumagalli, M., Cicalese, A., Piccinin, S., Gasparini, P., Luise, C., Schurra, C., Garre, M., Nuciforo, P.G., Bensimon, A.*, et al.* (2006). Oncogene-induced senescence is a DNA damage response triggered by DNA hyper-replication. Nature *444*, 638-642.

Diehl, F.F., Miettinen, T.P., Elbashir, R., Nabel, C.S., Darnell, A.M., Do, B.T., Manalis, S.R., Lewis, C.A., and Vander Heiden, M.G. (2022). Nucleotide imbalance decouples cell growth from cell proliferation. Nature cell biology *24*, 1252-1264.

Dok, R., Abbasi Asbagh, L., Van Limbergen, E.J., Sablina, A., and Nuyts, S. (2016). Nuclear p16INK4a expression predicts enhanced radiation response in head and neck cancers. Oncotarget *7*, 38785-38795.

Dok, R., Kalev, P., Van Limbergen, E.J., Asbagh, L.A., Vázquez, I., Hauben, E., Sablina, A., and Nuyts, S. (2014). p16INK4a impairs homologous recombination-mediated DNA repair in human papillomavirus-positive head and neck tumors. Cancer research *74*, 1739-1751.

Fung, C., Pupo, G.M., Scolyer, R.A., Kefford, R.F., and Rizos, H. (2013). p16(INK) (4a) deficiency promotes DNA hyper-replication and genetic instability in melanocytes. Pigment Cell Melanoma Res *26*, 236-246.

Gaillard, H., García-Muse, T., and Aguilera, A. (2015). Replication stress and cancer. Nature Reviews Cancer *15*, 276-289.

Hilton, B.A., Li, Z., Musich, P.R., Wang, H., Cartwright, B.M., Serrano, M., Zhou, X.Z., Lu, K.P., and Zou, Y. (2016). ATR Plays a Direct Antiapoptotic Role at Mitochondria, which Is Regulated by Prolyl Isomerase Pin1. Molecular cell *61*, 487.

Huang, Z., Chen, C.W., Buj, R., Tangudu, N.K., Fang, R.S., Leon, K.E., Dahl, E.S., Varner, E.L., von Krusenstiern, E., Cole, A.R.*, et al.* (2023). ATM inhibition drives metabolic adaptation via induction of macropinocytosis. J Cell Biol *222*.

Jeggo, P.A., Pearl, L.H., and Carr, A.M. (2016). DNA repair, genome stability and cancer: a historical perspective. Nature Reviews Cancer *16*, 35-42.

Lamm, N., Read, M.N., Nobis, M., Van Ly, D., Page, S.G., Masamsetti, V.P., Timpson, P., Biro, M., and Cesare, A.J. (2020). Nuclear F-actin counteracts nuclear deformation and promotes fork repair during replication stress. Nature cell biology *22*, 1460-1470.

Lim, C.Y., Davis, O.B., Shin, H.R., Zhang, J., Berdan, C.A., Jiang, X., Counihan, J.L., Ory, D.S., Nomura, D.K., and Zoncu, R. (2019). ER-lysosome contacts enable cholesterol sensing by mTORC1 and drive aberrant growth signalling in Niemann-Pick type C. Nature cell biology *21*, 1206-1218.

Liu, X., Lv, M., Zhang, W., and Zhan, Q. (2023). Dysregulation of cholesterol metabolism in cancer progression. Oncogene.

Longo, J., van Leeuwen, J.E., Elbaz, M., Branchard, E., and Penn, L.Z. (2020). Statins as Anticancer Agents in the Era of Precision Medicine. Clin Cancer Res *26*, 5791-5800.

Ma, Y., Vassetzky, Y., and Dokudovskaya, S. (2018). mTORC1 pathway in DNA damage response. Biochim Biophys Acta.

Manickavinayaham, S., Velez-Cruz, R., Biswas, A.K., Chen, J., Guo, R., and Johnson, D.G. (2020). The E2F1 transcription factor and RB tumor suppressor moonlight as DNA repair factors. Cell Cycle *19*, 2260-2269.

Maréchal, A., and Zou, L. (2013). DNA damage sensing by the ATM and ATR kinases. Cold Spring Harb Perspect Biol *5*.

Marshall, A.E., Roes, M.V., Passos, D.T., DeWeerd, M.C., Chaikovsky, A.C., Sage, J., Howlett, C.J., and Dick, F.A. (2019). RB1 Deletion in Retinoblastoma Protein Pathway-Disrupted Cells Results in DNA Damage and Cancer Progression. Mol Cell Biol *39*.

Minami, J.K., Morrow, D., Bayley, N.A., Fernandez, E.G., Salinas, J.J., Tse, C., Zhu, H., Su, B., Plawat, R., Jones, A.*, et al.* (2023). CDKN2A deletion remodels lipid metabolism to prime glioblastoma for ferroptosis. Cancer cell *41*, 1048-1060.e1049.

Molkentine, D.P., Molkentine, J.M., Bridges, K.A., Valdecanas, D.R., Dhawan, A., Bahri, R., Hefner, A.J., Kumar, M., Yang, L., Abdelhakiem, M.*, et al.* (2022). p16 Represses DNA Damage Repair via a Novel Ubiquitin-Dependent Signaling Cascade. Cancer research *82*, 916-928.

Orozco-Aguilar, J., Simon, F., and Cabello-Verrugio, C. (2021). Redox-Dependent Effects in the Physiopathological Role of Bile Acids. Oxidative medicine and cellular longevity *2021*, 4847941.

Postigo, A., Ramsden, A.E., Howell, M., and Way, M. (2017). Cytoplasmic ATR Activation Promotes Vaccinia Virus Genome Replication. Cell reports *19*, 1022-1032.

Primo, L.M.F., and Teixeira, L.K. (2019). DNA replication stress: oncogenes in the spotlight. Genetics and molecular biology *43*, e20190138.

Priya, B., Ravi, S., and Kirubakaran, S. (2023). Targeting ATM and ATR for cancer therapeutics: Inhibitors in clinic. Drug Discov Today *28*, 103662.

Saldivar, J.C., Cortez, D., and Cimprich, K.A. (2017). The essential kinase ATR: ensuring faithful duplication of a challenging genome. Nature reviews Molecular cell biology *18*, 622-636.

Sarkar-Agrawal, P., Vergilis, I., Sharpless, N.E., DePinho, R.A., and Rünger, T.M. (2004). Impaired processing of DNA photoproducts and ultraviolet hypermutability with loss of p16INK4a or p19ARF. J Natl Cancer Inst *96*, 1790-1793.

Saxton, R.A., and Sabatini, D.M. (2017). mTOR Signaling in Growth, Metabolism, and Disease. Cell *169*, 361-371.

Shi, Q., Chen, J., Zou, X., and Tang, X. (2022). Intracellular Cholesterol Synthesis and Transport. Frontiers in Cell and Developmental Biology *10*.

Shin, H.R., Citron, Y.R., Wang, L., Tribouillard, L., Goul, C.S., Stipp, R., Sugasawa, Y., Jain, A., Samson, N., Lim, C.Y.*, et al.* (2022). Lysosomal GPCR-like protein LYCHOS signals cholesterol sufficiency to mTORC1. Science (New York, NY) *377*, 1290-1298.

Tangudu, N.K., Buj, R., Wang, J., Cole, A.R., Uboveja, A., Fang, R., Amalric, A., Lyons, M.A., Chandran, U.R., and Aird, K.M. (2023). De novo purine metabolism is a metabolic vulnerability of cancers with low p16 expression. bioRxiv, 2023.2007.2015.549149.

Tramontano, A., Boffo, F.L., Russo, G., De Rosa, M., Iodice, I., and Pezone, A. (2020). Methylation of the Suppressor Gene p16INK4a: Mechanism and Consequences. Biomolecules *10*.

Turgeon, M.O., Perry, N.J.S., and Poulogiannis, G. (2018). DNA Damage, Repair, and Cancer Metabolism. Frontiers in oncology *8*, 15.

Uphoff, C.C., and Drexler, H.G. (2005). Detection of mycoplasma contaminations. Methods in molecular biology (Clifton, NJ) *290*, 13-23.

Vélez-Cruz, R., Manickavinayaham, S., Biswas, A.K., Clary, R.W., Premkumar, T., Cole, F., and Johnson, D.G. (2016). RB localizes to DNA double-strand breaks and promotes DNA end resection and homologous recombination through the recruitment of BRG1. Genes & development *30*, 2500-2512.

Wang, Y., Sharpless, N., and Chang, S. (2013). p16(INK4a) protects against dysfunctional telomere-induced ATR-dependent DNA damage responses. The Journal of clinical investigation *123*, 4489-4501.

Weber, A.M., and Ryan, A.J. (2015). ATM and ATR as therapeutic targets in cancer. Pharmacology & therapeutics *149*, 124-138.